Precipitation Microstructure in Different MJO Phases over Sumatra

Marzuki[a,*], Hiroyuki Hashiguchi[b], Toshiaki Kozu[c], Toyoshi Shimomai[c], Yoshiaki Shibagaki[d], Yukihiro Takahashi[e]

[a]*Department of Physics, Andalas University, Padang, Indonesia*
[b]*Research Institute for Sustainable Humanosphere (RISH), Kyoto University, Japan*
[c]*Interdisciplinary Faculty of Science and Engineering, Shimane University, Japan*
[d]*Dept. of Telecommunications and Computer Networks, Osaka Electro-Communication University, Japan*
[e]*Hokkaido University, Japan*

Abstract

Intraseasonal variation of precipitation and its microstructure are investigated using measurements from the Equatorial Atmospheric Radar (EAR) facility at Kototabang, west Sumatra, Indonesia (0.20^{o}S, 100.32^{o}E, 864 m above sea level). Raindrop size distribution (DSD) observations are obtained from a 2D-Video Disdrometer (2DVD) with a near continuous record of operation over eight consecutive years (2003-2010). Precipitation types are classified using 1.3-GHz wind profiler observation, and are partitioned according to active and inactive convective phase of Madden-Julian Oscillation (MJO). It is found that precipitation systems during the inactive phase are more continental in nature than those during the active phase. Cloud propagation from brightness temperature data indicates that Sumatra receives the rainfall mainly from maritime clouds during the active phase, whilst it is mainly from the continental clouds (land-based convection) during the inactive phase. Other facts of remarkable differences between active and inactive phase precipitation system are also observed from the vertical structure of precipitation. The precipitation during the inactive phase has a deeper storms, a higher reflectivity aloft, more lightning activity, more stratiform characteristics, as compared to the active phase. Assessment of cloud effective radius from the Moderate Resolution Imaging Spectroradiometer (MODIS) data also shows a slight difference in the cloud droplet between the active and the inactive MJO phases. Different convective storms in different MJO phase leads to different DSD characteristics and $Z - R$ relationships. Notably, on average, the DSD during the inactive phase tends to have a higher concentration of medium and large-size drops than the active counterpart, consistent with the previous study. Although the DSD parameters and coefficient of $Z - R$ relationships fall within the range of tropical maritime precipitation, the values for the deep convective rains during the inactive phase are somewhat larger than for maritime and closer to the continental cluster. Therefore, continental-like DSDs are somewhat dominant during the inactive phase, consistent with the intraseasonal variation of precipitation structure. The causative processes for the observed difference in DSD for the two phases have also been discussed with the help of satellite and radar data. Evaporation and updraft associated with the intense convection during the inactive phase seem to eliminate the small-sized drop from the spectra. Radar reflectivity during the inactive phase is larger than during the active MJO phase, at the same rainfall rate. This condition can limit the accuracy of radar-derived rainfall estimates over the tropics when applying a single $Z - R$ relation for the two MJO phases, particularly for deep convective rains.

Keywords:
Raindrop size distribution, Madden-Julian Oscillation, intraseasonal variation, cloud, Sumatra

1. Introduction

Rain microstructure, which is characterized by size distribution, shape and fall velocity of raindrop (e.g., Diederich et al., 2004; Thurai et al., 2009) has a broad list of applications in meteorology, hydrology, and related sciences. Long-term observation of raindrop size distribution (DSD) can be used to govern an equation between different rainfall variables such as radar reflectivity factor (Z)–rainfall rate (R) relationship. The equation is important to convert radar reflectivity from the weather radar to rainfall rate.

The DSD varies not only within a specific storm but also across differing storms types (e.g., Ulbrich , 1983; Tokay and Short, 1996) and climatic regimes (e.g., Bringi et al., 2003), which leads to the variability of $Z - R$ relation. Such variability substantially limits the accuracy of radar-derived rainfall estimates and becomes one of error source of rainfall estimates from the radar (Maki et al., 2005). Therefore, study of the DSD variability is important to improve the $Z - R$ conversion accuracy. Attempts to understand the variability of DSD have received considerable attention by measuring the DSD in various climatic regimes (e.g., Ulbrich , 1983; Tokay and Short, 1996; Bringi et al., 2003; Schönhuber et al., 2008; Marzuki et al. , 2013c). However, there still exist some fundamental issues which are poorly understood particularly for the tropical region where the variations of precipitation occur on a wide range of time-scales. Furthermore, the DSD measurement in the tropical region is still sparse.

The Madden–Julian Oscillation (MJO) is a dominant com-

*Corresponding author
Email address: marzuki@fmipa.unand.ac.id (Marzuki)

ponent of intraseasonal variability (30–60 days) over the tropics (Madden and Julian , 1971) and in some regions can have immense societal and economic impacts. It involves variation in several parameters such as wind, sea surface temperature, cloudiness, and rainfall. Detailed reviews of the MJO can be found in Madden and Julian (1994) and Zhang (2005). Although there have been many studies on the role of the MJO in the rainfall variability over the tropics (e.g., Seo and Kim , 2003; Matthews and Li , 2005; De Souza and Ambrizzi , 2006; Rauniyar and Walsh, 2011; Oh et al. , 2012), its impact on the rain microstructure such as DSD has not been described in detail. Kozu et al. (2005) found a difference in the DSD of two phases of MJO during the first campaign of Coupling Processes in the Equatorial Atmosphere (CPEA) project at Kototabang, west Sumatera, Indonesia (Fig. 1). Marzuki et al. (2010b) analyzed the same data as Kozu et al. (2005) but with a better rain classification. Both studies found that the DSD during the convectively inactive is broader than that during active MJO phases, particularly for heavy rain ($R > 10$ mm h^{-1}). It was coincident with higher radar reflectivity during the inactive than during the active phases, at the same rainfall rate.

Wheeler and Hendon (2004) defined eight MJO phases that correspond to the positions of the centre of the convective activity along the tropics. Both Kozu et al. (2005) and Marzuki et al. (2010b) analyzed one month data that cover only one MJO cycle. Further advances must be made in order to improve our overall understanding on the natural variability of rain microstructure in response to the MJO. In this paper, the DSD data from disdrometer measurement with a near continuous record of operation over eight consecutive years (2003-2010) at Kototabang, west Sumatra, are analyzed. Prior to the discussion of the DSD in section 3, the data and method are introduced in section 2. General features of precipitation and atmospheric circulation for each MJO phase is first discussed in section 3. Section 4 addresses the discussion of the results, and section 5 is a summary that includes recommendations for a future work.

2. Data and methods

2.1. Raindrop size distribution measurement

A 2D-Video Disdrometer (2DVD) was used to measure drop size, shape, and fall speed. The method to obtain the DSD from such drop data is explained in detail by Schönhuber et al. (2008). The 2DVD has been collecting samples of raindrop spectra almost continuously over eight years (2003–2010). The performance of our instrument can be found in Marzuki et al. (2013a). The 2DVD occasionally records spurious small drops especially in heavy rainfall that may be due to the mismatching problem between the front-and side-view camera images. Such problem can be reduced by re-matching the data from the standard matching software with the camera data (Marzuki et al., 2013a). However, the camera data are not available for the entire experimental period. Therefore, a threshold of drop fall speed was adopted to filter out the spurious drops using Gunn and Kinzer (GK) observation results (Gunn and Kinzer , 1949), as proposed by Tokay et al. (2001). We retained the drops within 65% of GK observations. The comparison of rainfall rate derived from the filtered data and that obtained by optical rain gauge (ORG) is very good (figure not shown). The DSDs for two-minute intervals, adopting a 0.2 mm channel interval (Marzuki et al. , 2010a) from 0.4 mm to 10.25 mm were constructed. This criterion may also reduce the spurious drops.The drops in excess 10 mm are presumably not real drops (Marzuki et al., 2013a). We also disregarded very light rain (R <0.1 mm h^{-1}).

After collection, the disdrometer data were processed to calculate the DSD parameters and $Z - R$ relationship. To reduce statistical and quantization errors, the DSD parameters were only estimated from minute DSD having more than 4 consecutive bins with non-zero values. The DSD is parameterized by the normalized gamma distribution function(e.g., Testud et al. , 2001; Bringi et al., 2003). Liquid water content (LWC) is used to normalize the measured DSD. The DSD parameters such as normalized intercept parameter (N_w), mass-weighted mean diameter (D_m) and shape parameter (μ) can be estimated from raindrop spectra by first calculating LWC, D_m, σ_m, and then μ as follow

$$LWC = \frac{\pi.10^{-3}}{6}\int_0^{\infty} D^3 N(D) dD, \tag{1}$$

$$D_m = \frac{\int_0^{\infty} D^4 N(D)\, dD}{\int_0^{\infty} D^3 N(D)\, dD}, \tag{2}$$

$$N_w = \frac{4^4}{\pi\rho_w}\frac{LWC}{D_m^4}, \tag{3}$$

$$\sigma_m = \sqrt{\frac{\int_0^{D_{max}} (D - D_m)^2 D^3 N(D)\, \mathrm{d}D}{\int_0^{D_{max}} D^3 N(D)\, \mathrm{d}D}}, \tag{4}$$

$$\mu = \left(\frac{\sigma_m}{D_m}\right)^2 - 4, \tag{5}$$

where ρ_w is water density.

Rainfall rate R (mm h^{-1}) is expressed in terms of the DSD as follow

$$R = 6\pi.10^{-4}\int_0^{\infty} D^3 v(D) N(D) dD, \tag{6}$$

where $v(D)$ is the raindrop fall speed in still air and is approximated by the empirical form as (Atlas et al., 1973),

$$v(D) = 9.65 - 10.3e^{(-0.6D)}(\rho/\rho_0)^{0.4}, \tag{7}$$

where ρ_0 and ρ are the air densities at sea level and at altitude of 864 m above sea level, respectively. In similar fashion with R, radar reflectivity factor Z (mm^6 m^{-3}) can be expressed as

$$Z = \int_0^{\infty} D^6 N(D) dD. \tag{8}$$

For weather radar application, the DSD is important to derive $Z - R$ equation ($Z = AR^b$). In this work, the equation was estimated by linear regression R over Z on log-transformed values. A group of 10 DSDs samples of sequential R was averaged to minimize the effect of the spurious variability on disdrometric data (Lee and Zawadzki, 2005).

2.2. Radars

Precipitation is often partitioned into convective or stratiform types because different rain types have different $Z - R$ relation and latent heating profile. For this study, the classification was based on six years (2004-2009) of 1.3 GHz boundary layer radar (BLR) observation. The radar was operated about 300 m away from the 2DVD site. The characteristics and performance of this instrument can be found in Gage et al. (1994) and Renggono et al. (2001). The radar echoes were assumed as precipitation if rain at the ground was detected by the 2DVD with the intensity larger than 0.1 mm h^{-1}. Furthermore, to ensure that both instruments are simultaneously observing rain, only the echoes having the radar reflectivity and Doppler velocities greater than 18 dBZ and 3 m s^{-1}, respectively, were analyzed (Renggono et al., 2001). Rains are partitioned into stratifrom, mixed stratiform/convective, deep and shallow convectives, by slightly modifying the algorithm proposed by Williams et al. (1995). The classification was performed using 2-min averaged radar reflectivity, Doppler velocity and spectral width.

The evolution of rain drop spectra with height is useful to interpret the characteristics of surface DSD. Vertical air motions and the effects of turbulence on the raindrop for each MJO phase are observed from 47 MHz Equatorial Atmosphere Radar (EAR) data. The vertical profile of DSD parameters are estimated using 24 GHz micro rain radar (MRR) data. Simultaneous observation of MRR and 2DVD are not available. The data are only available from 2011 to 2012. The characteristics and performance of EAR and MRR are provided in detail by Fukao et al. (2003) and Peters and Andersson (2002), respectively. Table 1 summarizes the system specification of radars used in this work.

2.3. Satellite data

The National Centers for Environmental Prediction (NCEP) Department of Energy (DOE) reanalysis II dataset (Kanamitsu et al., 2002) and the National Oceanic and Atmospheric Administration (NOAA) interpolated outgoing longwave radiation (OLR) data (Liebmann and Smith , 1996) were used to calculate the MJO index. The data are also used to identify the location of deep convection and to observe the weather variables around Sumatra for each MJO phase.

Ten years of brightness temperature data (2001-2010) from geostationary satellites which are operated by the Japan Meteorological Agency, were used to study the diurnal cycle of convective cloud around Sumatra. The data are interpolated to a 0.2° x 0.2° grid to calculate percent high cloudiness (PHC) for the temperature of 230K or less (PHC_{230}), as in Marzuki et al. (2013b). To determine the cloud properties over Kototabang, daily MODerate resolution Imaging Spectroradiometer (MODIS) data onboard Terra and Aqua satellites for three years of observation (2007-2009) were used.

2.4. Lightning data

Convective clouds of large vertical extent are very often accompanied by lightning and thunder (Petersen and Rutledge , 1998). Three years (2007-2009) of the World Wide Lightning Location Network (WWLLN) data were used to produce temporal distribution of cloud to ground lightning over Kototabang. The WWLLN provides real time lightning locations around the globe by operating a network of lightning location sensors at very low frequency (Rodger et al., 2004).

2.5. Classification of MJO phases

To examine the characteristics of rain microstructure in response to MJO, it is necessary to define the MJO phase. The amplitude and phase of the MJO are determined by using the Real-time Multivariate MJO (RMM) index proposed by Wheeler and Hendon (2004). The index is constructed by the two leading principal component time series (RMM1 and RMM2) of the empirical orthogonal functions of the near–equatorial (15°S–15 °N) daily zonal winds at 850 and 200 hPa, as well as the OLR. The index that has amplitude greater than one is assumed as strong MJO, vice versa, the condition is defined as weak MJO. In this study, we focused only on strong MJO case because the weather variables during weak MJO are very close to the climatology (Rauniyar and Walsh, 2011). The MJO phase space is divided into eight sectors corresponding to the positions of the centre of the convective activity along the tropics. Since there are not enough observations of rainfall to composite the intraseasonal cycle for the eight individual phases of the MJO particularly for simultaneous observation of BLR and 2DVD, the data are instead classified into just two categories, i.e., active and inactive (suppressed) MJO phases. The active convective phase of the MJO (hereafter active MJO) for Kototabang and nearby locations occurs in phases 2, 3, 4, and 5, and the suppressed convective phase of the MJO (hereafter inactive MJO) occurs in phases 1, 6, 7 and 8.

3. Results

3.1. General features of precipitation cycle

The diurnal cycle of percent high cloudiness (PHC_{230}) in a geographic framework is illustrated in Figs. 2 and 3, for active and suppressed MJO phases, respectively. The intraseasonal difference in the diurnal cycle of PHC_{230} around Sumatera are very clear both over open ocean and land. During the active MJO phase over the Indian Ocean, PHC_{230} exhibit a nocturnal peak, indicating the peak of organized mesoscale convective systems (Chen and Houze, 1997). This oceanic convection system moves eastward and reaches Sumatra island at 13 local time (LT). Large value of PHC_{230} over Sumatra lasted until 02 LT (next day), as also clearly observed from the weather radar (Fig. 4).

The duration of cold cloud over Sumatra during the inactive is shorter than during the active phases. The large value of PHC_{230} during the inactive phase lasted only until 24 LT, as also observed from the weather radar (Fig. 5). A peak of convective development circa 15-16 LT (Fig. 5) indicates the rapid organization of convection from interactions among sea breezes and moist convection in close proximity. By local midnight (Fig. 5), land-based convection enters a dissipation phase

and seaward movement was evident. Convection of continental origin moves to the coast of west Sumatra and the complete dissipation of land-based convection occurs at 06 LT. It is plausible to assume that precipitation systems over Sumatra during the inactive phase are more continental in nature than those during the active phase. However, both active and inactive phases precipitation systems developed initially over north slopes of a meridionally oriented mountain range. Therefore, the orographic effect may also contribute to the precipitation system over Sumatra (Shibagaki et al. , 2006).

To further illustrate several of the previous points, Fig. 6 exhibits the diurnal cycle of lightning and surface rainfall rate at Kototabang. Note that the lightning data are only from three years of WWLLN observation (2007-2009). During such period, the number of strokes during the inactive and the active phases are 24415 and 11587, respectively. Therefore, the stroke during the inactive is twice as frequent as during the active phases. This lightning characteristics is coincident with the mean rainfall rate (Fig. 6d) in which during the inactive phase mean rainfall intensity is higher than during the active one. This finding strengthens the assumption based on the cloud propagation (Figs. 2-5) in which precipitation system during the inactive phase are more continental in nature than those during the active phase.

Figure 6b shows the diurnal cycle of surface rainfall data. Of eight years observation (2003-2010), 94267 and 59768 1-min rain data ($R > 0.1$ mm/h) are recorded during the active and the inactive MJO phases, respectively. Total rainfall for such data number are 5176 and 4303 mm, correspondingly. Ratio of active to the inactive rain profile is about 1.6, but the ratio for rain total is only 1.2. Thus, convective storms are more intense but shorter duration during the inactive than during active phases. Furthermore, this also indicates that well organized convective clouds are mostly accompanied by a larger component of stratiform during the active phase, whilst isolated convective clouds are dominant during the inactive MJO phase. During 2004-2009, we have 843 days of BLR observation that can be used to investigate the rain type dependence of vertical structure. It was found that the number of stratiform rains increases during the active MJO phase with the ratio of active to inactive profile being approximately 1.3 (3344/2618 2-min). The same as stratfiform, the number of shallow convective rains also increases during the active phase with the ratio of 1.5 (4965/3319 2-min). In contrast, deep convective rains suppress during the active MJO with the ratio of 0.7 (427/643 2-min). Although the peak of precipitation occurrence for the two phases are observed at different time (16 LT for the inactive and 16-22 LT for the active phases), the peak of total rainfall accumulation for the two phases is the same, i.e, at 16 LT (Fig. 6c). This indicates that the most intense convective for the two phases occurs at 16 LT (Figs. 7-8). However, storms producing heavy rain differ intraseasonally in terms of vertical structure. During the inactive phase, they tend to be a little deeper, and have higher reflectivities aloft, than during active phase.

3.2. Average drop size distributions

During the entire experimental period (2003-2010), 57224 1-min precipitation DSDs meet the quality control mentioned above. Figure 9a compares the DSD during the inactive and the active MJO phases obtained by averaging all instant DSDs during the entire experimental period. The DSD with a rain rate of 3 mm h^{-1} and 30 mm h^{-1} were extracted and used for the averaging. These rain rates are often used as typical values representing light and heavy rain rates (Kozu et al., 2006). Notably, on average, the DSD during the inactive phases tends to have a higher concentration of medium and large-size drops ($D > 3$ mm) than the active counterpart. On the other hand, the DSD during the active phase has more small raindrops with $D < 2$ mm. The evidence of intraseasonal variation of DSD become more obvious during heavy rain.

Simultaneous observation of 2DVD and 1.3-GHz wind profiler were only available during 2004-2009. The observation produced a dataset consisting of 5114 spectra from stratiform, 2647 from shallow convective, 1136 spectra from deep convective and 135 spectra from mixed stratiform/convective rains (2-min aggregation windows). To examine the characteristics of the DSD between the active and inactive MJO pahses, the DSD measurements were averaged for the specific rain type. Because of the limited data, no averaging was performed for mix-stratiform. To further discern the difference of the DSD between the active and inactive phases, the observed DSD for each rain type are further stratified into two classes according to their rain rates. Since there are not enough observations of rainfall to composite the rain type cycle for 30 mm h^{-1}, the DSDs having a rain rate of 5 mm h^{-1}, 3 and 15 mm h^{-1} are used for the average of stratiform (Fig. 9b), deep and shallow convective (Fig. 9c-d), respectively. The number of DSD samples for the aforementioned rain classes is more than 100 for light rain and more than 10 for heavy rain. A difference in the spectra could be seen from the convective rains in which during the inactive phase the concentration of medium and large-size drops are higher. As was inferred from the entire experimental period (Fig. 9a) , the evidence of intraseasonal variation of convective DSD become more obvious during the heavy rain. The intraseasonal differences appeared in the range of $\log_{10}N(D) \sim$ 100 or less.

The composite DSD during the active phase were much narrower than Marshall-Palmer (MP) distribution (Marshall and Palmer , 1948), particularly for heavy rain. Kozu et al. (2005) investigated the difference between a measured radar reflectivity in dB and that from the MP radar reflectivity and it was called as $\triangle Z_{MP}$. They found that during the active MJO, $\triangle Z_{MP}$ are generally negative, indicating that DSDs are narrow, consistent with the characteristics of long data record used in this study. Marzuki et al. (2010b) provided a comprehensive follow-up of Kozu et al. (2005) and found that intrasesonal variation of DSD was clearly observed at convective and heavy rains, as also seen in Fig. 9.

3.3. N_w-D_m Relationship

Figure 10 shows the histograms of the DSD parameter for each rain type during the inactive and active MJO phases. We

only consider the spectra having μ in the range from -3 to 30 as in Marzuki et al. (2013a). To compare the current result with the DSD data from diverse climates, the composite statistics of D_m and N_w along with the data of Bringi et al. (2003) is given in Fig. 11. Note that Bringi et al. (2003) classified stratiform-convective rains based on a simple rain threshold. Therefore, some convective rains can be classified as stratiform, or vice versa. As can be observed from the figures, the histogram of the DSD parameter during the inactive is slightly different from that of active phase. In general during the inactive phase the histogram of D_m more skews toward the low value and the histogram of μ and N_w more skew toward the high value than during the inactive phases. The mean value of μ for active (inactive) phase for stratiform, shallow and deep convective rains are 9.36 (8.17), 14.72 (12.92) and 10.71 (8.52), respectively.

Bringi et al. (2003) found that, on average, the scatter of $< N_w >$ and $< D_m >$ of stratiform fell almost on a straight line. The value of our stratiform rain events for all MJO phases are also close to that line (Fig. Fig. 11b). The mean values of D_m and N_w (marked as 7-8) are $D_m \sim 1.28$ (1.38) and $N_w \sim 3.58$ (3.32), respectively. These D_m values are close to those at tropical/maritime precipitation system. However, the N_w for the inactive phase is close to continental Colorado (marked as 6).

For the convective rain, the result of Bringi et al. (2003) formed two clusters that corresponded roughly to maritime and continental precipitation systems. The mean values of D_m and N_w for the active (inactive) MJO phases, for deep convective rains are 1.49 (1.85) and 4.11 (3.82), respectively. Furthermore, the values for shallow convective rains are 1.28 (1.58) and 4.37 (4.04), correspondingly. Thus, the data points are concentrated around $1 < D_m < 2$ mm, and matched with the maritime convective cluster. This is not very surprising because KT is located in maritime continent region which is surrounded by ocean. Although D_m value is close to the tropical maritime (marked as 1-5), the N_w is lower than those found in the tropical maritime precipitation but Papua. Moreover, the values for deep convective during the inactive MJO (marked as 11) are somewhat larger than maritime-cluster. Therefore, continental-like DSDs are somewhat dominant during the inactive phase, consistent with the general feature of precipitation discussed in Section 3.1.

3.4. Implications for remote sensing

One of the most important application of the DSD measurement is for rainfall estimation from a weather radar through the $Z-R$ relations ($Z = AR^b$). For the entire dataset (2003-2010, 1-min DSD records), the relation was calculated as $Z = 250R^{1.40}$. The default equation of Next Generation of Weather Radar (NEXRAD) is $Z = 300R^{1.40}$ (Fulton et al., 1998). However, for tropical environments Rosenfeld et al. (1993) recommended an alternate relationship ($Z = 250R^{1.40}$). Therefore, b-coefficient exponent over Sumatra is the same as that utilized by the standard NEXRAD $Z - R$, but the intercept coefficient $A = 250$ is lower. Furthermore, b-coefficient exponent over Sumatra is lower than that recommended by Rosenfeld et al. (1993) for tropical rainfall event, but the intercept coefficient $A = 250$ is the same.

Figure 12 contains the partitioning of the $Z - R$ relations according to the MJO phases and rain type. The relation for all dataset of stratiform rains is $Z = 279R^{1.32}$, or $Z = 278R^{1.40}$ for a fixed $b = 1.4$. The relations of stratiform rain according to MJO phases are $Z = 259R^{1.29}$ (active) and $Z = 316R^{1.38}$ (inactive phase), respectively. These relationships mapped to $Z = 258R^{1.40}$ and $Z = 316R^{1.40}$ if adhering to a fixed b coefficient. Under deep convective condition, the relationships according to the active and inactive MJO phases are calculated as $Z = 177R^{1.34}$ and $Z = 279R^{1.44}$, respectively. For the fixed b coefficient, these relationships mapped to $Z = 173R^{1.40}$ and $Z = 294R^{1.40}$. All dataset of deep convective rains are associated with $Z = 226R^{1.44}$, or $Z = 234R^{1.40}$. The relationship for shallow convective during the active and inactive MJO phases are $Z = 163R^{1.33}$ and $Z = 201R^{1.43}$, respectively. These correspond to $Z = 161R^{1.40}$ and $Z = 203R^{1.40}$ when applying a fixed b-coefficient estimate. All dataset of shallow convective revealed the equation of $Z = 179R^{1.38}$, or $Z = 178R^{1.40}$ for the fixed b coefficient.

As highlighted in Fig. 12, the radar reflectivity is higher during the inactive than during the active MJO phases, for the same rainfall rate. This is consistent with the characteristics of surface DSD in which the inactive (active) conditions exhibit larger (smaller) number concentrations associated with larger drop sizes. Although the DSD spectra during the inactive phase is closer to the continental cluster than during the active phase (Fig. 11), estimated $Z - R$ intercept coefficient is different from those reported for continental locations such as Sauvageot and Lacaux (1995) for Continental ($Z = 364R^{1.36}$) and equatorial Africa ($Z = 369R^{1.28}$), Ochou et al. (2007) for Congo ($Z = 389R^{1.34}$). On the other hand, the coefficients fall within the range of previous study over tropical maritime region such as Tokay and Short (1996) for Darwin ($Z = 315R^{1.20}$) and $Z = 232R^{1.38}$ of Maki et al. (2001). This result is not surprising because KT is located in a maritime continent region surrounded by the ocean. However, it can be seen clearly from this study that continental-like DSDs are somewhat dominant during the inactive MJO phase that leads to the larger radar reflectivity during the inactive phase, for the same rainfall rate. Thus, the usage of a single $Z - R$ relation will underestimate rainfall rate in one phase and overestimate in the other phase.

4. Discussions

This section discusses the possible microphysical process affecting the characteristics of DSD found in the previous section. First, the possible effect of evaporation is explored. The evaporation will result in a greater loss of the number of small diameter particles (Rosenfeld and Ulbrich, 2003). Figure 13 shows the probability density functions of 18-dBZ echo tops for stratiform and deep convective rains during the active and the inactive MJO phases. The number of occurrences per 150 m is normalized by all occurrences in all height bins, and expressed as a percentage. The value of 18 dBZ is close to the minimum detectable signal of the BLR (Renggono et al., 2001).

When the backscattered signal is very strong, the profiler receiver has a nonlinear response so that strong echo at the bright band level are sometimes reduced (e.g., Ralph, 1995; Marzuki et al., 2013a). Relatively large or numerous hydrometeors are found high above the freezing level, particularly for stratiform rains during the inactive phase. Furthermore, a surface rain rate during the inactive phase are associated with low-level evaporation. In general, the evaporation is suggested by the more frequent occurrence of higher reflectivities above 6 km, as compared to levels closer to the ground. Low level evaporation is significantly observed only for stratiform, as also pointed out by Liu and Fu (2001). High solar radiation and ground temperature during the inactive phase (Kozu et al. , 2005), may favour for evaporation of small-sized drops. Consequently a deficit of small raindrops in the inactive phase were slightly observed (Fig. 9). A consequence of evaporation is the decrease of N_W and it can be seen clearly from Fig. 11. Another consequence is the increase of A (Rosenfeld and Ulbrich, 2003), as observed in Fig. 12.

To further compare and contrast the typical microphysical process for large-sized drops in the two MJO phases, we examine the CFAD of reflectivity. As can be seen in Eq. (8), Z is an inherent property of the drop size distribution. Z is proportional to the 6^{th} power of the drop sizes, so larger drops make for much more reflectivity than small drops. Therefore, downward increasing or decreasing of radar reflectivity is closely related to the evolution of raindrop, particularly large-size drop(e.g., Schumacher and Houze , 2003; Thurai et al., 2003). Figure 14 shows the CFAD of reflectivity for each rain type. Although it is not uniform, in general, we found that the gradient of mean CFAD for stratiform during the inactive (active) phase is -0.38 (-0.22 dBZ/km), and for deep convective is 1.0 (0.87 dBZ/km). A bit larger downward increasing of deep convective reflectivity during the inactive phase indicates low-level raindrop growth by collision-coalescence. Furthermore, a bit larger downward decreasing of stratiform reflectivity during the inactive phase indicates low-level raindrop elimination by evaporation (Liu and Fu , 2001).

Marzuki et al. (2010b) provided the vertical profile of DSD from the EAR measurement during the CPEA-I. They found significant downward increasing of large-sized drop during the inactive phase which is coincident with the reflectivity gradient, as found in the current work. For closer look at the raindrop evolution, the CFAD of the DSD parameter estimated from the MRR measurement is given in Fig. 15. It can be seen from the figure, the mean vertical profile of N_W during the active phase is larger than during the inactive phase, particularly for stratiform rains consistent with the surface DSD (Figs. 9-11). The MRR measurement is only available to 4 km so that we can not separate deep and shallow convective rains. A slightly difference in the mean of D_m profile is also observed. Downward increasing gradients of D_m during active (inactive) for stratiform and convective rains are 0.06 (0.10 mm/km) and 0.26 (0.31 mm/km), respectively. Therefore, larger sized-raindrop growth during the inactive is more significant than during the active phase.

Orographically controlled precipitation systems may be significant at KT, particularly during the active MJO phases (Shibagaki et al. , 2006). Shallow orographic precipitation would have many small raindrops (Rosenfeld and Ulbrich, 2003), as in Fig. 11a (marked as 12). Other factors that influence the DSD during their fall is updraft and downdraft. These processes can dramatically generate collision and eliminates the small-sized drop from the spectra at the lower levels(Rosenfeld and Ulbrich, 2003). We examine the possible upward and downward currents using the EAR measurement (Fig. 16). Although the vertical profile of vertical wind are concentrated around ± 0.4 m/s, the intraseasonal variation of vertical wind can be observed during the deep convective rains in which a bit stronger vertical wind (> 0.4 m/s) is more frequent during the inactive phase. Thus, the vertical structure of precipitation during the inactive phase tend to be deeper, have higher reflectivities aloft, and seems to be more frequent associated with strong vertical wind, as compared to the active phase. A relationship of reflectivity profile and vertical wind have been previously investigated by Mori et al. (2006), using the data during the CPEA-I. Therefore, this upward current may also decrease the concentration of small drops during the inactive phase.

To further explore the contrast of cloud properties for the two MJO phases, the histogram of cloud effective radius (r_e) from MODIS data for three years (2007-2009) is given in Fig. 17. Mean r_e for ice during active phase is approximately 24.7 μm, while 26.2 μm for the inactive phase. On the other hand, mean r_e for liquid water during active phase is approximately 19.4 μm, while 18.6 μm for the inactive phase. King et al. (2003) found that cloud effective particle radius of liquid water clouds is significantly larger over ocean than land. Intraseasonal variation of land-ocean contrast can be seen clearly from the mode r_e value. The values for liquid water and ice during active (inactive) phases are 15.9 (14.4 μm) and 20.3 (16.9 μm), respectively. Such values are larger than that found by King et al. (2003), but it is obvious that the value during the active phase is closer to the maritime cloud property than during the inactive phase. On the other hand, the value during the inactive phase is closer to the continental cloud property. This cloud property contrast is consistent with the characteristics of the DSD discussed above.

5. Conclusions

The present study reinforces the previous finding on the intraseasonal variation of precipitation microstructure over Sumatra. The precipitation systems during the inactive phase are more continental in nature than those during the active phase. Although the DSD parameters and coefficient of $Z-R$ relationships fall within the range of tropical maritime precipitation, the values for deep convective during the inactive phase are somewhat larger than for maritime and closer to the continental cluster. Thus, continental-like DSDs are somewhat dominant during the inactive phase, consistent with the intraseasonal variation of precipitation structure. Intense convective system during the inactive phase is associated with the raindrop spectra having a larger concentration of large-sized drop. As consequence, radar reflectivity during the inactive phase is larger than during the active MJO phase, at the same rainfall rate. This condition

can limit the accuracy of radar-derived rainfall estimates over the tropics when applying a single $Z - R$ relation for the two MJO phases, particularly for deep convective rains. Therefore, this study can be additional reference for ongoing effort to improve the DSD and $Z - R$ models for the radar measurement of equatorial rainfall.

Radar reflectivity (Z) is an inherent property of the drop size distribution so that downward increasing or decreasing of Z is closely related to the evolution of raindrop, particularly large-size. The general pattern of the vertical structure of Z over Indonesian Maritime Continent in different MJO phase using Tropical Rainfall Measuring Mission (TRMM) 2A25 radar reflectivities profile and a wind profiler network along equatorial Indonesia is being investigated and will be published in subsequent paper. Furthermore, a comprehensive study regarding the maritime and continental cloud property contrast for the two MJO phases should be also pursued in the future.

Acknowledgements

The observations of Equatorial Atmospheric Radar (EAR) facility are supported by Grant-Aid for Scientific Research on Priority Areas funded by the Ministry of Education, Culture, Sports, Science, and Technology (MEXT) of Japan. This study was partially supported by Collaborative Research based on Equatorial Atmosphere Radar (EAR). The authors wish to recognize the substantial discussion and data of V. N. Bringi of Colorado State University.

References

Atlas, D., Srivastava, R. C. and Sekhon, R. S., 1973. Doppler radar characteristics of precipitation at vertical incidence. Rev. Geophys. Space Phys. 11, 1–35.

Bringi, V. N., Chandrasekar, V., Hubbert, J., Gorgucci, E., Randeu, W. L. and Schoenhuber, M., 2003. Raindrop size distribution in different climatic regimes from disdrometer and dual-polarized radar analysis. J. Atmos.Sci. 60, 354–365.

Chen, S. S., Houze, R. A. Jr., 1997. Diurnal variation of deep convective systems over the tropical Pacific warm pool. Quart. J. Roy. Meteor. Soc. 123, 357-388.

De Souza, E. B. and Ambrizzi, T., 2006. Modulation of the intraseasonal rainfall over tropical Brazil by the Madden Julian oscillation. Int. J. Climatol. 26, 1759–1776, doi: 10.1002/joc.1331.

Diederich, M., Crewell,S., Simmer, C. and Uijlenhoet, R., 2004. Investigation of rainfall microstructure and variability using vertically pointing radar and disdrometer. Proc. ERAD. 80–86.

Fulton, R. A., Breidenbach, J. P., Seo, D. J., Miller, D. A. and OBannon, T., 1998. The WSR-88D Rainfall Algorithm. Wea. Forecasting, 13, 377-395, doi: http://dx.doi.org/10.1175/1520-0434(1998)013¡0377:TWRA¿2.0.CO;2

Fukao, S., Hashiguchi, H., Yamamoto, M., Tsuda, T., Nakamura, T., Yamamoto, M. K., Sato, T., Hagio, M. and Yabugaki, Y., 2003. The Equatorial Atmosphere Radar (EAR): System Description and First Results. Radio Sci., 38(4), 1053, doi:10.1029/2002RS002767.

Gage, K.S., Williams, C.R. and Ecklund, W.L., 1994. UHF wind profilers: A new tool for diagnosing tropical convective cloud system. Bull. Am. Meteorol. Soc. 75, 2289–2294.

Gunn, R. and Kinzer, G., 1949. The terminal velocity of fall for water droplets in stagnant air, J. Meteorol. 14, 243–248.

Kanamitsu, M., Ebisuzaki, W., Woollen, J., Yang, S-K., Hnilo, J. J., Fiorino, M., Potter, G. L., 2002. NCEPDOE AMIP-II Reanalysis (R-2), Bull. Amer. Meteor. Soc. 83:11, 1631–1643

King, M., Menzel, W., Kaufman, Y., Tanre, D., Gao, B., Platnick, S., Ackerman, S., Remer, L., Pincus, R., and Hubanks, P., 2003. Cloud and aerosol properties, precipitable water, and profiles of temperature and water vapor from MODIS, IEEE Trans. Geosci. Remote Sens. 41, 442-458.

Kozu, T., Shimomai, T., Akramin, Z., Marzuki, Shibagaki,Y., and Hashiguchi, H., 2005. Intraseasonal variation of raindrop size distribution at Koto Tabang, West Sumatra, Indonesia. Geophys. Res. Lett. 32, L07803, 10.1029/2004GL022340.

Kozu, T., Reddy, K. K., Mori, S., Thurai, M., Ong, J. T., Rao, D. N., and Shimomai, T., 2006. Seasonal and diurnal variations of raindrop size distribution in Asian monsoon region. J. Meteorol. Soc. Japan. 84A, 195-209.

Lee, G. and Zawadzki, I., 2005. Variability of drop size distributions : Noise and noise filtering in disdrometric data. J. Appl. Meteorol. 44, 634–652.

Liebmann B. and Smith, C.A., 1996. Description of a Complete (Interpolated) Outgoing Longwave Radiation Dataset. Bull. Amer. Meteor. Soc. 77, 1275–1277.

Liu, G. and Fu, Y., 2001. The Characteristics of Tropical Precipitation Profiles As Inferred From Satellite Radar Measurements. J. Meteorol. Soc. Japan, 79, 131–143.

Madden, R. A. and Julian, P. R., 1971. Detections of a 40-50 day oscillation in the zonal wind in tropical Pacific. J. Atmos. Sci. 28, 702–708.

Madden, R. A. and Julian, P. R., 1994. Observations of the 40-50 day tropical oscillation: a review. Mon. Wea. Rev. 122, 814–837.

Maki, M., Keenan, T. D., Sasaki, Y. and Nakamura, K., 2001. Characteristics of the Raindrop Size Distribution in Tropical Continental Squall Lines Observed in Darwin, Australia. J. Appl. Meteor. 40, 1393-1412. doi: http://dx.doi.org/10.1175/1520-0450(2001)040¡1393:COTRSD¿2.0.CO;2

Maki, M., Park, S.G., and Bringi, V.N., 2005. Effect of natural variations in raindrop size distributions on rain rate estimators of 3 cm wavelength polarimetric radar. J. Meteorol. Soc.Japan. 83, 871–893.

Matthews, A. J. and Li, H. Y. Y., 2005. Modulation of station rainfall over the western Pacific by the Madden-Julian oscillation. Geophys. Res. Lett. 32 (14), L14827.

Marshall, J. S. and Palmer, W. Mc K., 1948. The distribution of raindrops with size. J. Meteor. 5, 165-166. doi: http://dx.doi.org/10.1175/1520-0469(1948)005¡0165:TDORWS¿2.0.CO;2

Marzuki, Randeu, W.L., Schoenhuber, M., Bringi, V.N., Kozu, T. and Shimomai, T., 2010a. Raindrop size distribution parameters of disdrometer data with different bin sizes, IEEE Trans. Geosci. Remote Sens. 48, 3075–3080.

Marzuki, Kozu, T., Shimomai, T., Randeu, W.L., Hashiguchi, H. and Vonnisa, M., 2010b. Raindrop size distributions of convective rain over equatorial Indonesia during the first CPEA campaign, Atmos. Research. 96, 645–655.

Marzuki, Randeu, W.L., Kozu, T., Shimomai, T., Hashiguchi, H. and Schoenhuber, M., 2013a. Raindrop axis ratios, fall velocities and size distribution over Sumatra from 2D-Video Disdrometer measurement, Atmos. Research. 119, 23-37.

Marzuki,Hashiguchi, H., Yamamoto, M. K., Yamamoto, M., Mori, S., Yamanaka, M.D., Carbone, R. E., Tuttle, J.D., 2013b. Cloud episode propagation over the Indonesian Maritime Continent from 10 years of infrared brightness temperature observations, Atmos. Research. 120, 268–286.

Marzuki, M., Hashiguchi, H., Yamamoto, M. K., Mori, S., and Yamanaka, M. D., 2013c. Regional variability of raindrop size distribution over Indonesia, Ann. Geophys. 31, 1941-1948, doi:10.5194/angeo-31-1941-2013.

Mori, S., Hamada, J.-I., Yamanaka, M. D., Kodama, Y.-M., Kawashima, M., Shimomai, T., Shibagaki, Y., Hashiguchi, H. and Sribimawati, T., 2006. Vertical wind characteristics in precipitating cloud systems over west Sumatera, Indonesia, observed with equatorial atmosphere radar: Case study of 2324 April 2004 during the first CPEA campaign period. J. Meteor. Soc. Japan. 84A, 113-131.

Peters, G., and Andersson, T., 2002. Rain observations with a vertically looking Micro Rain Radar (MRR), Bor. Environ. Res. 7, 353–362.

Petersen, W. A. and Rutledge, S. A., 1998. On the relationship between cloud-to-ground lightning and convective rainfall. J. Geophys. Res., 103, 14025–14040.

Oh J., Kim, K. and Lim, G., 2012. Impact of MJO on the diurnal cycle of rainfall over the western Maritime Continent in the austral summer. Clim Dyn. 38, 1167-1180.

Ochou, A. D., Nzekou, A. and Sauvageot, H., 2007. Parameterization of drop size distribution with rain rate. Atmos. Res. 84, 58-66.

Ralph, M.F., 1995. Using radar-measured radial vertical velocities to distinguish precipitation scattering from clear-air scattering. J. Atmos. Oceanic

Technol. 12, 257–267.
Rauniyar, S. P., Walsh, K. J. E., 2011. Scale Interaction of the Diurnal Cycle of Rainfall over the Maritime Continent and Australia: Influence of the MJO. J. Climate, 24, 325–348.
Renggono, F., Hashiguchi, H., Fukao, S., Yamanaka, M.D., Ogino, S.Y., Okamoto, N., Murata, F., Sitorus, B.P., Kusdy, M., Kartasasmita, M. and Ibrahim, G., 2001. Precipitating clouds observed by 1.3-GHz boundary layer radars in equatorial Indonesia, Ann. Geophys., 19, 889–897.
Rodger, C. J., Brundell, J. B., Dowden, R. L. and Thomson, N. R., 2004. Location accuracy of long distance VLF lightning locationnetwork, Ann. Geophys. 22, 747758, doi:10.5194/angeo-22-747-2004.
Rosenfeld, D., Wolff, D. and Atlas, D., 1993. General probability-matched relations between radar reflectivity and rain rate. J. Appl. Meteor. 32, 50-72.
Rosenfeld, D. and Ulbrich, C. W., 2003. Cloud microphysical properties, processes, and rainfall estimation opportunities. Radar and Atmospheric Science: A collection of Essays in Honor of David Atlas, Meteorol. Monogr. 52, 237–258.
Sauvageot, H. and Lacaux, J. P., 1995. The shape of averaged drop size distributions, J. Atmos. Sci., 52, 10701083.
Shibagaki, Y., Kozu, T., Shimomai, T., Mori, S., Murata, F., Fujiyoshi, Y., Hashiguchi, H. and Fukao, S., 2006. Evolution of a super cloud cluster and the associated wind fields observed over the Indonesian Maritime Continent during the first CPEA campaign. J. Meteorol. Soc. Japan. 84A, 19–31.
Schönhuber, M., Lammer, G., and Randeu, W. L., 2008. The 2-D-Video-Disdrometer, in: Michaelides, S. (Eds.) Precipitation: Advances in Measurement, Estimation and Prediction. Springer, ISBN: 978-3-540-77654-3.
Schumacher, C. and Houze, R. A., 2003. Stratiform rain in the tropics as seen by the TRMM precipitation radar. J. Climate. 16, 1739–1756.
Seo, K.-H. and Kim, K.-Y, 2003. Propagation and initiation mechanisms of the Madden-Julian oscillation, J. Geophys. Res. 108, 4384, doi:10.1029/2002JD002876.
bibitem[Rauniyar and Walsh (2011)]Rauniyar2011 Rauniyar, S. P. and Walsh, J. E. K., 2011. Scale Interaction of the Diurnal Cycle of Rainfall over the Maritime Continent and Australia: Influence of the MJO. J. Climate, 24, 325-348.
Thurai, M., Iguchi, T., Kozu, T., Eastment, J. D., Wilson, C. L., and Ong, J. T., 2003. Radar observation in Singapore and their implications for the TRMM precipitation radar retrievel algorithms, Radio Sci. 38, doi:10.1029/2002RS002855.
Thurai, M., Bringi, V. N. and Petersen, W. A., 2009. Rain microstructure retrievals using 2-D video disdrometer and C-band polarimetric radar, Adv. Geosci. 20, 13–18.
Testud, J., Oury, S., Black, R. A., Amayenc, P. and Dou, X., 2001. The concept of normalized distributions to describe raindrop spectra: A tool for cloud physics and cloud remote sensing. J. Appl. Meteorol. 40, 1118–1140.
Tokay, A. and Short, D. A., 1996. Evidence from tropical raindrop spectra of the origin of rain from stratiform versus convective clouds. J. Appl. Meteorol. 35, 355–371.
Tokay, A., Kruger, A. and Krajewski, W. F., 2001. Comparison of drop size distribution measurements by impact and optical disdrometer. J. Appl. Meteorol. 40, 2083–2097.
Ulbrich, C. W., 1983. Natural variations in the analytical form of raindrop size distributions. J. Clim. Appl. Meteorol. 22, 1764–1775.
Wheeler M. C. and Hendon H. H., 2004. An all-season real-time multivariate MJO index: Development of an index for monitoring and prediction. Mon. Wea. Rev. 132, 1917–1932.
Williams, C. R., Ecklund, W. L. and Gage, K. S., 1995. Classification of precipitating clouds in the tropics using 915-MHz wind profilers. J. Atmos. Oceanic Technol. 12, 996–1011.
Zhang, C., 2005. Madden-Julian Oscillation. Rev. Geophys. 43(2), 1–36.

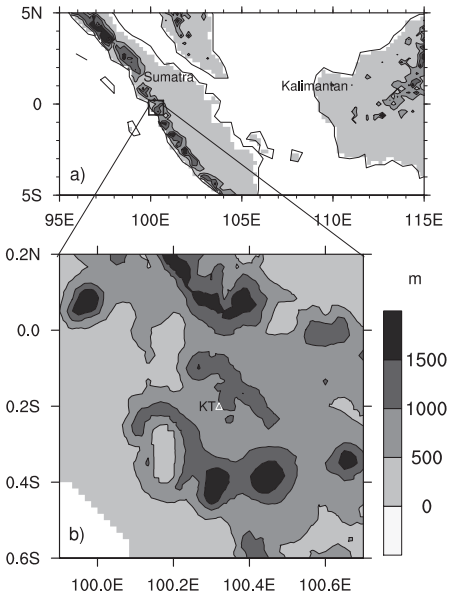

Figure 1: Topographic features in meter unit around Sumatra (a) and Kototabang abbreviated by KT (b).

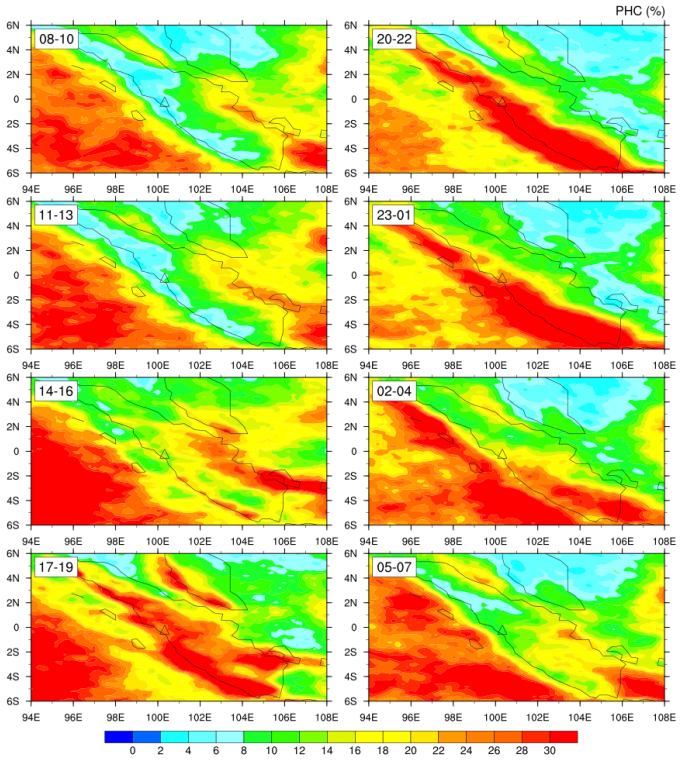

Figure 2: Diurnal cycle of PHC_{230} during the active MJO phase, △ denotes Kototabang.

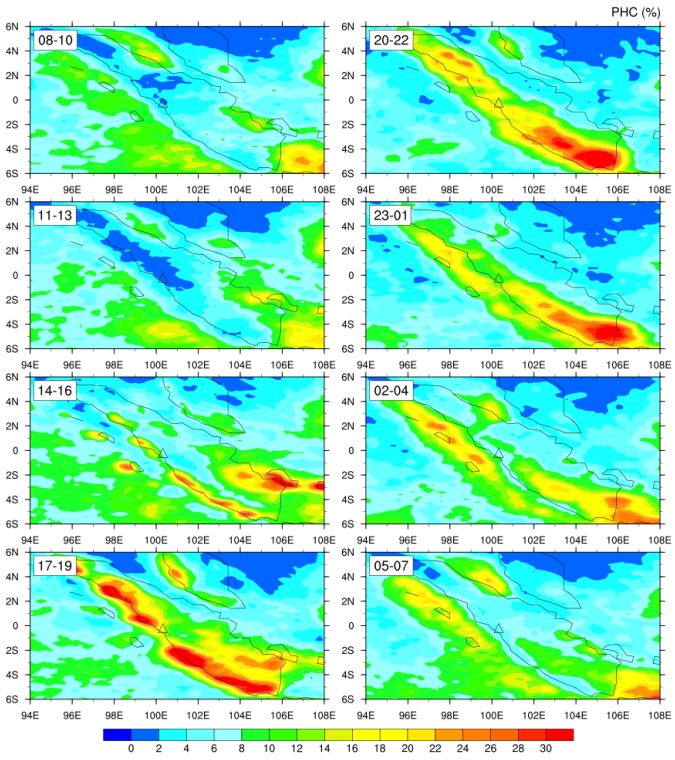

Figure 3: Same as Fig. 2 but for the inactive MJO phase.

Table 1: Radar specifications

Radar Parameters	1.3-GHz BLR	EAR	MRR	Weather radar
Radar system	Pulse	Pulse	FMCW	Pulse
Operating frequency	1.3 GHz	47.0 MHz	24 GHz	9.74 GHz
Transmit power	1.1 kW	100 kW	50 mW	40 kW
Antenna	5.9 m^2	110 m in diameter	60 cm in diameter	1.2 m in diameter
Beam width	4.1^o	3.4^o	2^o	-
Range resolution	150 m	150 m	150 m	0.25 km
Observation period	2004-2009	2003-2010	2011-2012	2004-2010

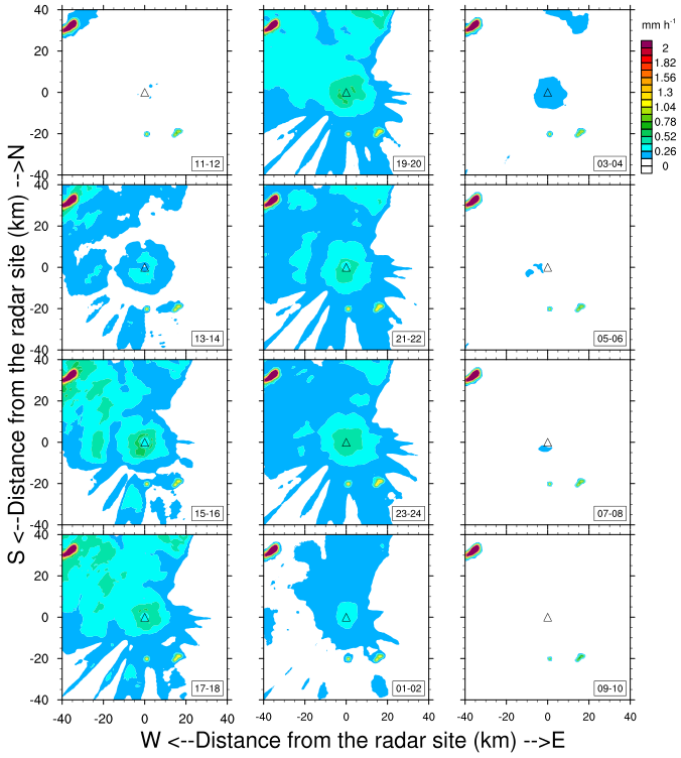

Figure 4: Diurnal cycle of horizonal distribution of precipitation at 2.1 km height derived from constant altitude plan position indicator (CAPPI) observation of X-band weather radar during the active MJO phase from 2004 to 2010. Radar reflectivity was simply converted to rainfall rate using the MP model.

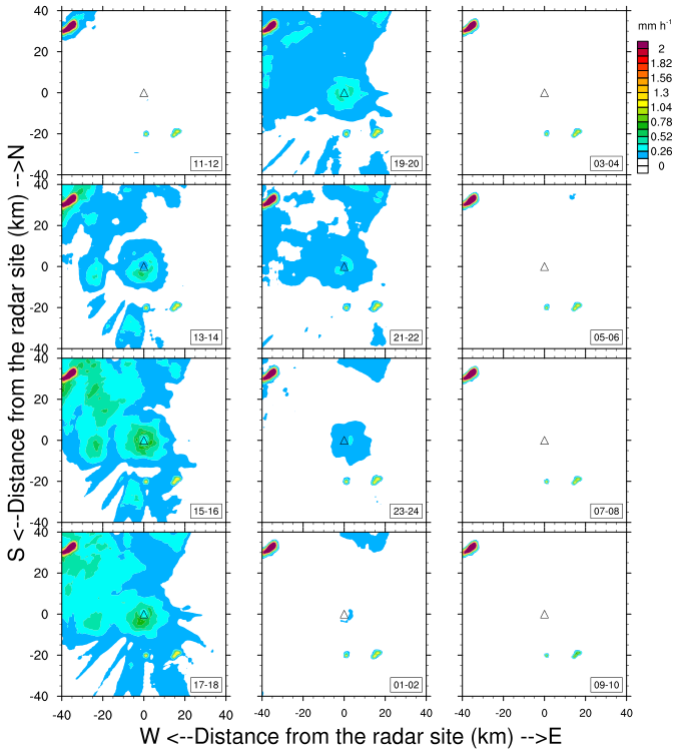

Figure 5: Same as Fig. 4 but for the inactive MJO phase.

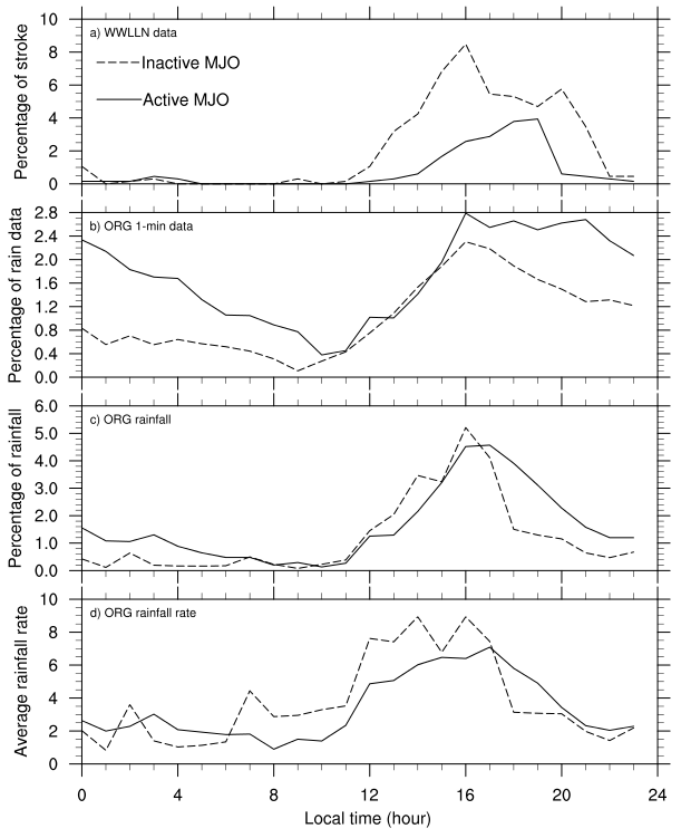

Figure 6: The diurnal variation of lightning and the rainfall at KT (a-c) as well as average rainfall rate (d). The percentage expressed in the figures are relative to the total number of profiles and the rainfall accumulation.

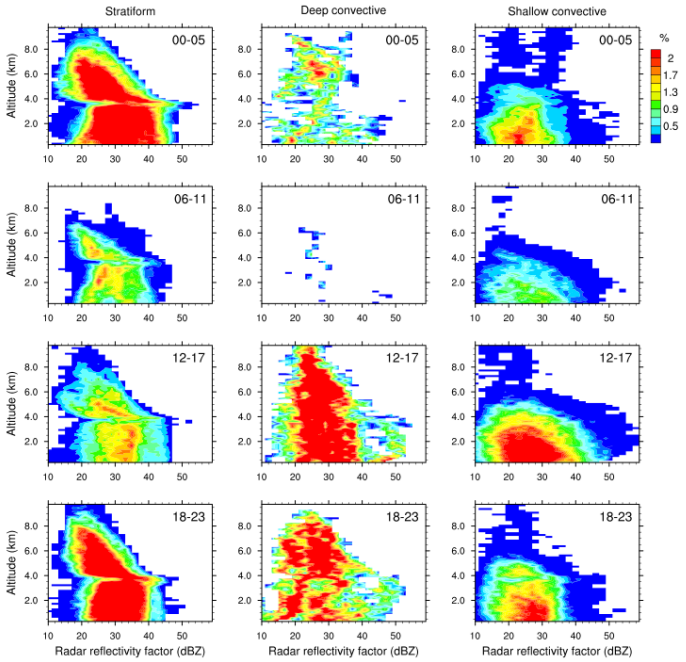

Figure 7: Contoured frequency with altitude diagram (CFAD) of radar reflectivity from 1.3 GHz wind profiler observation during the active MJO phase from 2004 to 2009, on a diurnal basis.

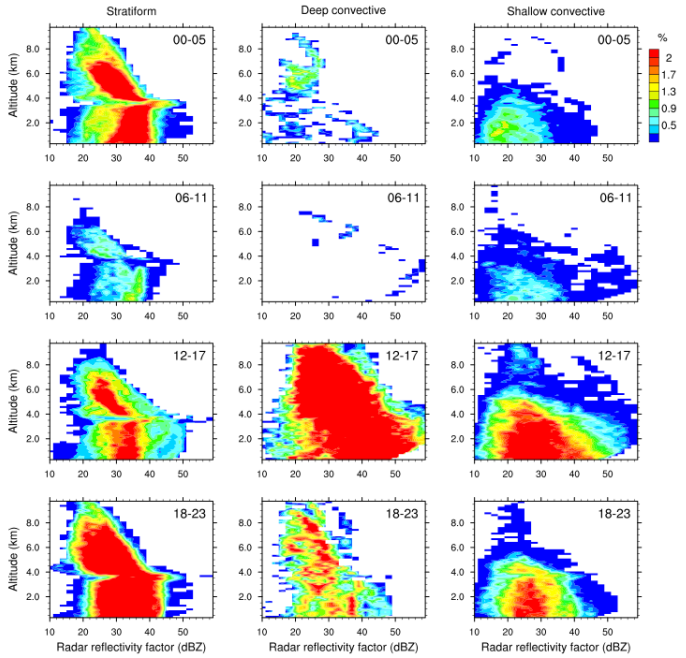

Figure 8: Same as Fig. 7 but for the inactive MJO phase.

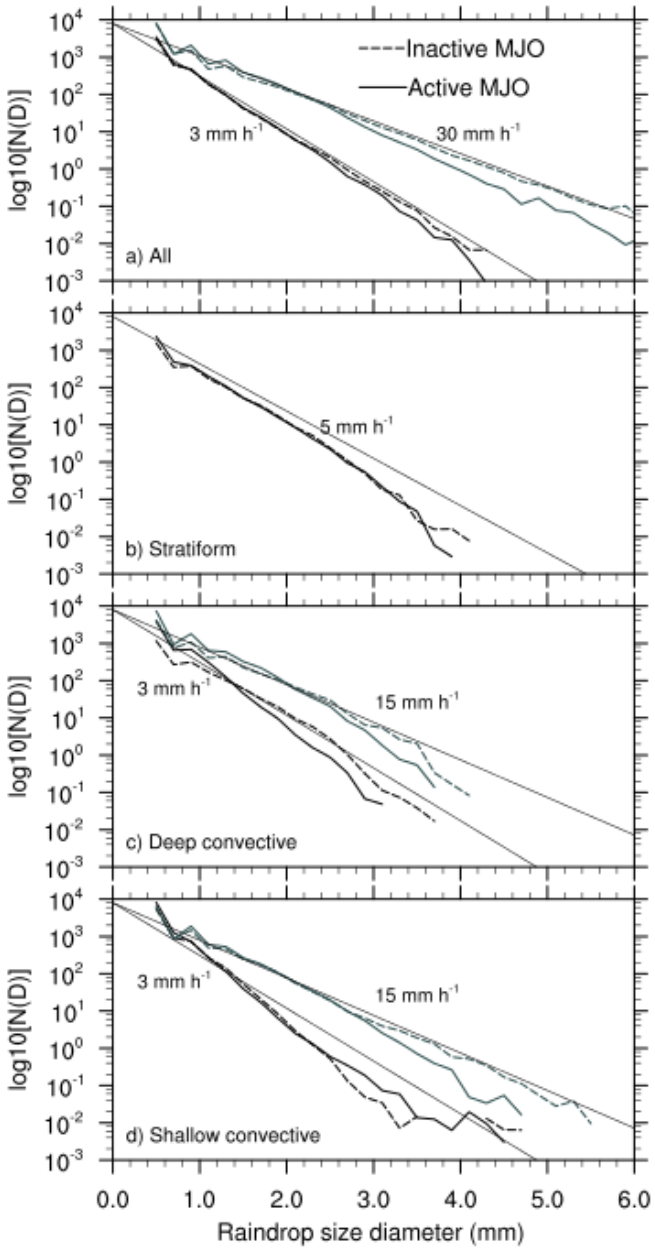

Figure 9: Averaged DSDs for the entire experimental period (2003-2010) partitioned into 3 mm h^{-1} and 30 mm h^{-1} (a) and for simultaneous observation of 2DVD and 1.3-GHz wind profiler during 2004-2009 (b-d). The representative MP model distribution for each rain intensity is indicated by grayed solid line.

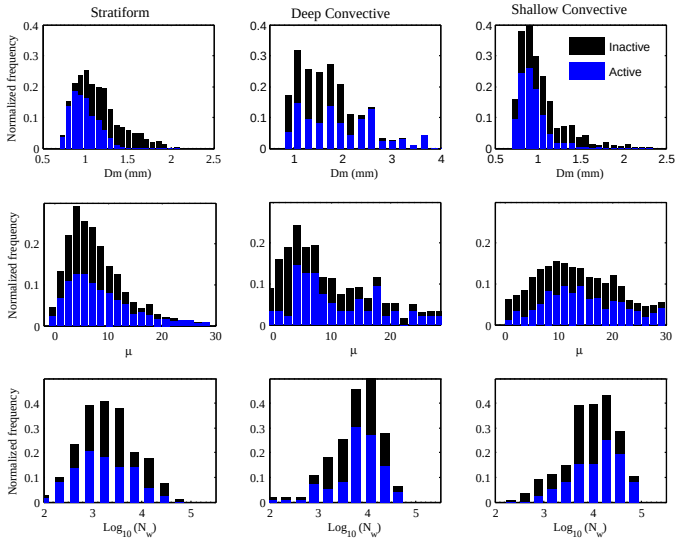

Figure 10: Histograms of relative distributions of D_m, $\log_{10}N_w$ and μ for stratiform, deep and shallow convective classified into the active and the inactive MJO phases.

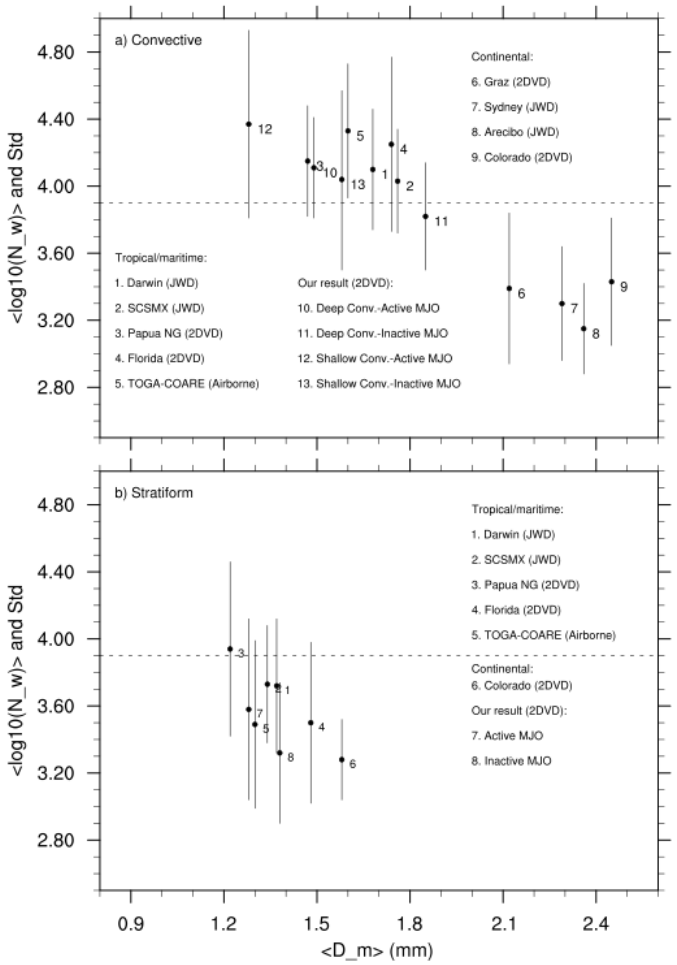

Figure 11: Mean $\log_{10}N_w$ (with $\pm$ 1σ standard deviation) vs mean D_m on intraseasonal and precipitation type basis. Dashed line is the Marshall-Palmer value ($\log_{10}N_w$ = 3.9).

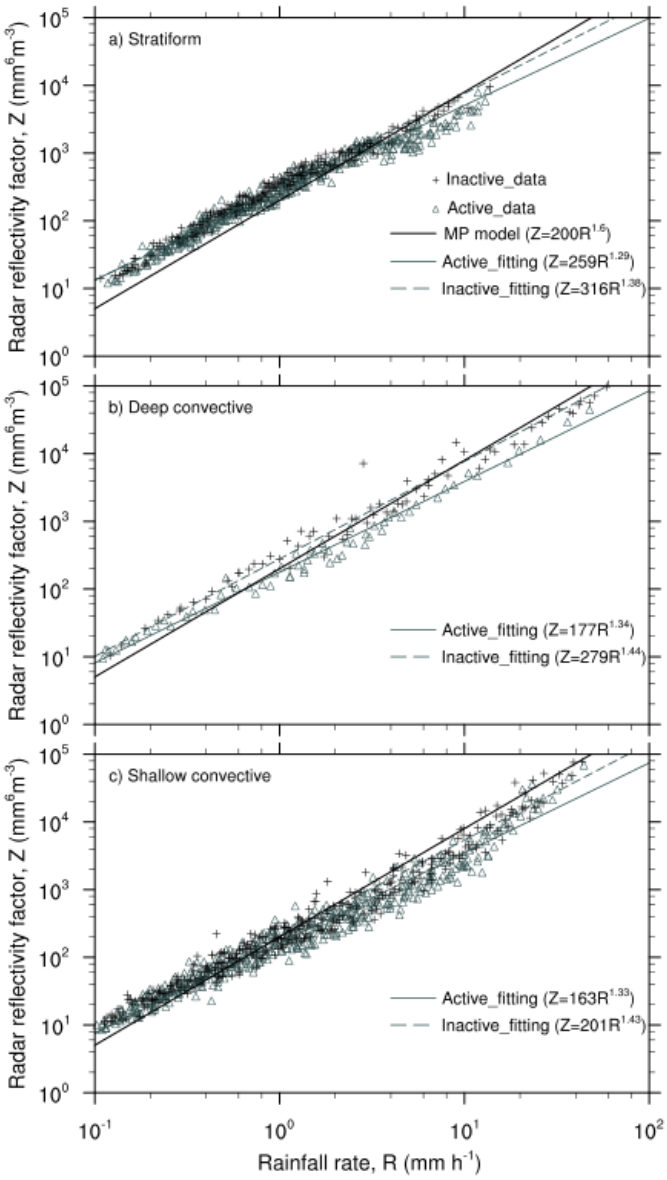

Figure 12: $Z - R$ relationship for stratiform, deep and shallow convective rains during the active and inactive MJO phases, along with the MP model.

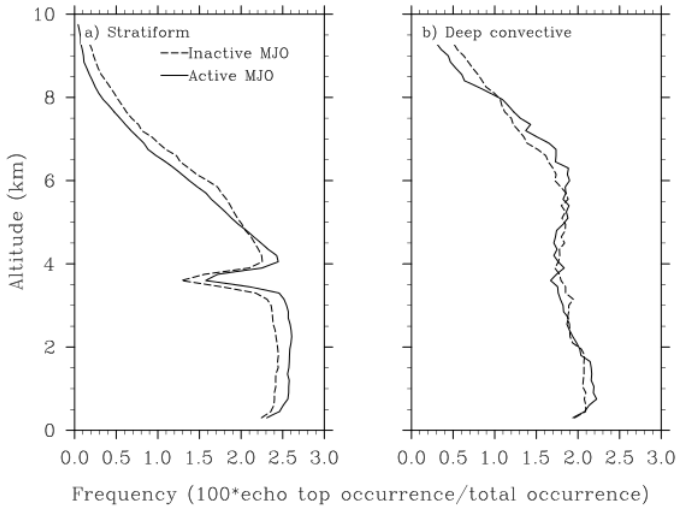

Figure 13: Probability density functions of 18-dBZ echo tops for stratiform and deep convective rains during active and inactive MJO phases. The number of occurrences per 150 m is normalized by all occurrences in all height bins, and expressed as a percentage.

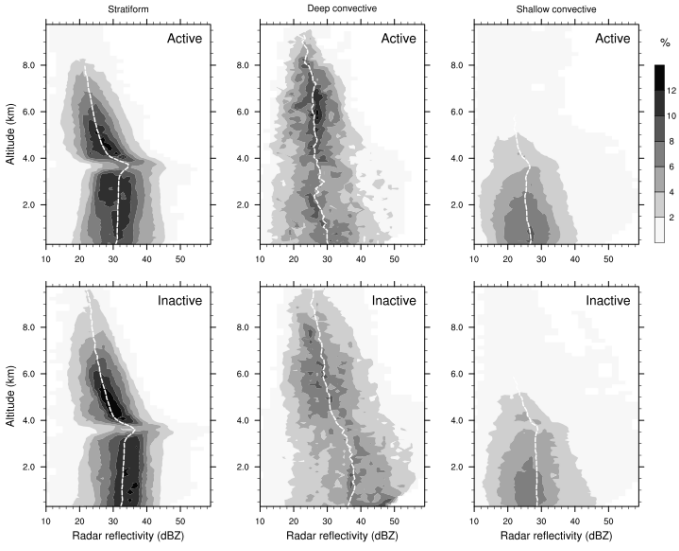

Figure 14: Same as Fig. 7 but for the entire dataset of the inactive and the active MJO phase and for each rain type. Mean values are denoted by white lines.

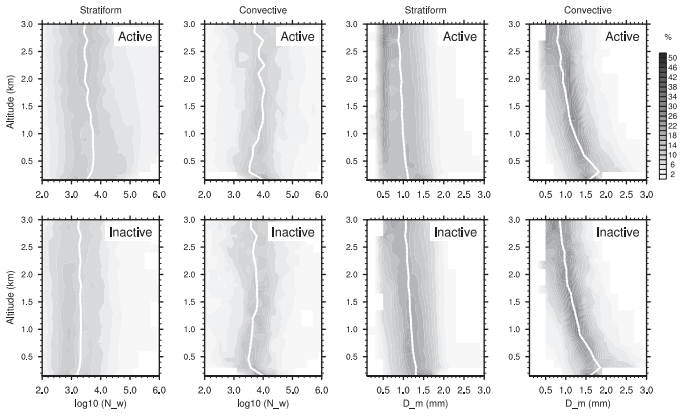

Figure 15: The CFAD of $\log_{10}N_w$ and D_m from the MRR measurement during active and inactive MJO phases for stratiform and convective rains. Mean values are denoted by white lines. The data are from the period of 2011-2012.

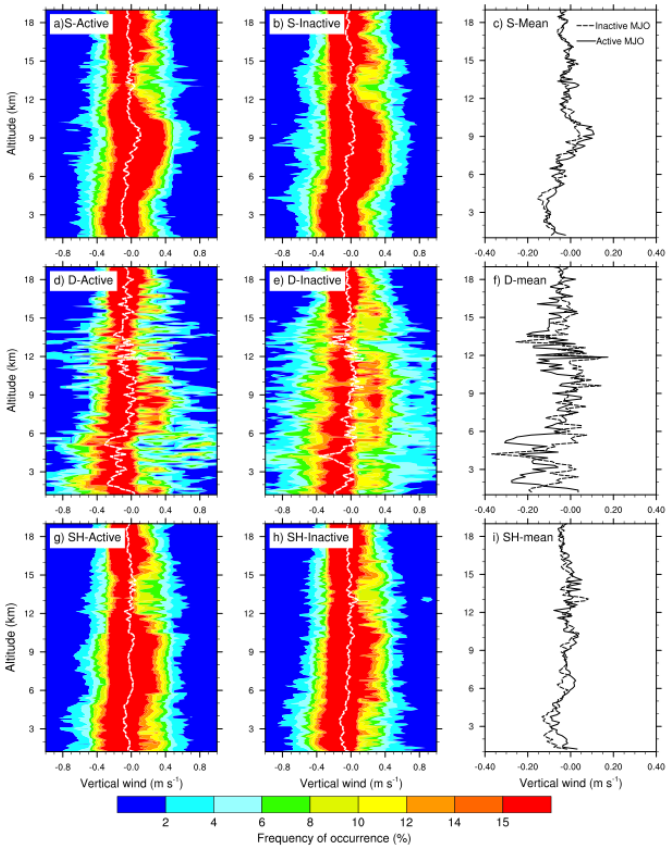

Figure 16: The CFAD of vertical wind obtained from the EAR measurement during active (left) and inactive (middle) MJO phases for a specific rain type. Mean vertical winds are given at the right side. The data are from the period of 2004-2010.

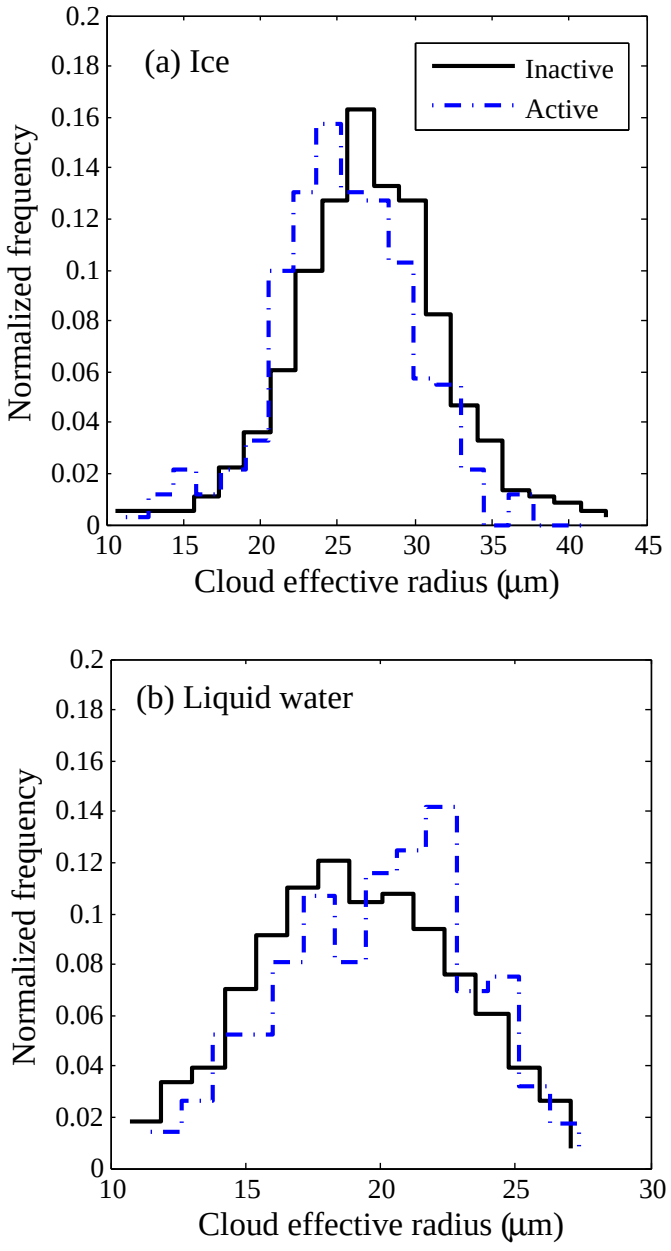

Figure 17: Histograms of relative distributions of cloud effective radius of liquid water and ice clouds classified into the active and the inactive MJO phases.